Axis-Displaced Dual-Reflector Antennas for Omnidirectional Coverage With Arbitrary Main-Beam Direction in the Elevation Plane

Fernando José da Silva Moreira, *Member, IEEE*, and José Ricardo Bergmann, *Member, IEEE*

***Abstract*—The synthesis of classical dual-reflector antennas suited to provide omnidirectional coverages with arbitrary main-beam direction in the elevation plane is discussed. Both sub- and main reflectors are bodies of revolution generated by axis-displaced conic sections, so to transform a spherical radiation emanating from the antenna principal focus (at the symmetry axis) into an equiphase field distribution over a conical aperture. Closed-form design equations are presented for the geometric-optics synthesis of all possible configurations. Several case studies are investigated and analyzed by the accurate method of moments technique in order to validate the proposed design procedure.**

***Index Terms*—Axis-displaced reflector antennas, omnidirectional antennas, reflector antennas.**

I. Introduction

THE growing interest on high-speed Internet access for residential and small business costumers has created a demand for last mile broadband access. In this scenario, when compared with wired technologies, broadband wireless technologies show lower costs, rapid deployment, and lower maintenance and upgrade costs. Among wireless services, the Local Multipoint Distribution Service (LMDS) offers a method of access to broadband interactive services, where a centralized hub, or base station, simultaneously communicates with many fixed subscribers in the vicinity of the hub. To avoid spectral congestion and to provide new services in urban centers, LMDS is proposed to operate at frequencies above 26 GHz. However, at microwave and millimeter-wave bands, system operation requires clear line-of-sight (LOS) links between the hub station and the subscribers, suggesting the deployment of base-station antennas above potential customers on either a tall tower or on the rooftop of a tall building. At the customer premises, roof-mounted directional antennas provide the necessary LOS links. However, to obtain an adequate illumination of the covered area, avoid interference in adjacent systems, and, consequently, increase spectral efficiency, it may be desirable to use a base-station antenna with an omnidirectional (or sectorized) coverage in the azimuthal plane with a main-beam downward tilt in the elevation plane.

Manuscript received March 9, 2006; revised May 26, 2006. This work was supported in part by CNPq and FAPERJ, Brazil.

F. J. da Silva Moreira is with the Department of Electronics Engineering of the Federal University of Minas Gerais, 30161-970 Belo Horizonte, MG, Brazil.

J. R. Bergmann is with the Center for Telecommunications Studies of the Catholic University, 22453-900 Rio de Janeiro, RJ, Brazil.

Digital Object Identifier 10.1109/TAP.2006.882181

Wireless communication links at relatively high frequencies (up to millimeter waves) make attractive the use of compact reflector antennas, capable of providing wider absolute bandwidths necessary to transmit wideband signals and, thus, encompassing several services. Single- and dual-reflector antennas have been investigated for omnidirectional coverage in the azimuthal plane. The reflector surfaces are bodies of revolution obtained by spinning confocal conic sections or shaped generating curves about a common symmetry axis [1]–[5]. As demonstrated in [4], the dual-reflector antenna leads to more compact designs than the single reflector concept, as the dual configuration requires a considerably smaller reflector diameter to achieve the necessary aperture width for adequate control of the vertical radiation pattern. Although this analysis was developed for designs with a main-beam direction along the horizon, the conclusions are still valid for main-beam tilts up to 30° below the horizon. Besides the compactness, the use of axis-displaced dual-reflector configurations offers the additional advantage of controlling the feed return loss by minimizing the subreflector radiation toward the feed horn, as discussed in [6]–[8].

For more efficient coverage of LMDS scenarios, it may be desirable to impose a uniform field amplitude across the coverage area by employing antennas with a cosecant-squared radiation pattern, with its peak placed below the horizon to avoid interference [3], [5]. To attain the desired uniform coverage, a dual-reflector arrangement could be shaped by applying an iterative optimization procedure associated with a diffractive analysis, where a starting solution is essential to ensure fast numerical convergence. Classical axis-displaced conic sections with main-beam direction below horizon can provide an efficient starting solution for shaping procedures, as well as an adequate control of the antenna geometric parameters to avoid blockage and minimize the feed return loss [6]–[8].

In this paper, we explore axis-displaced dual-reflector configurations to provide omnidirectional coverage with an arbitrary main-beam direction in the elevation plane, thus extending the investigations conducted in [4]–[8]. By applying geometric optics (GO) principles, closed-form equations for the classical dual-reflector antenna design are derived and discussed in Section II. Four different antenna configuration are identified and distinguished by two different options for the ray mapping (from the focus to the antenna aperture) and by the location of the subreflector caustics, similarly to the discussion in [7] and [8]. The design procedure is exemplified

0018-926X/$20.00 © 2006 IEEE

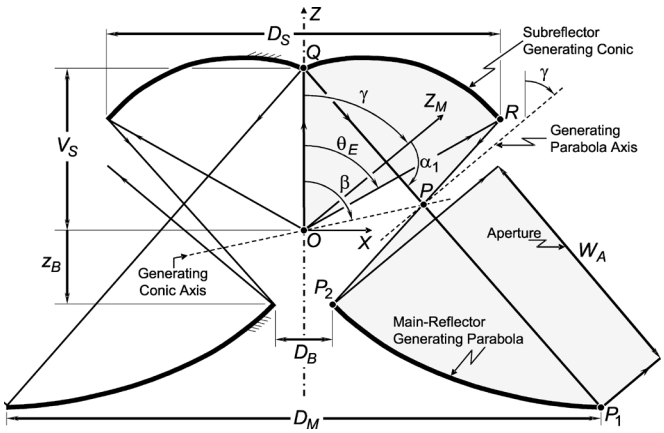

Fig. 1. Basic parameters of an omnidirectional dual-reflector system for option I.

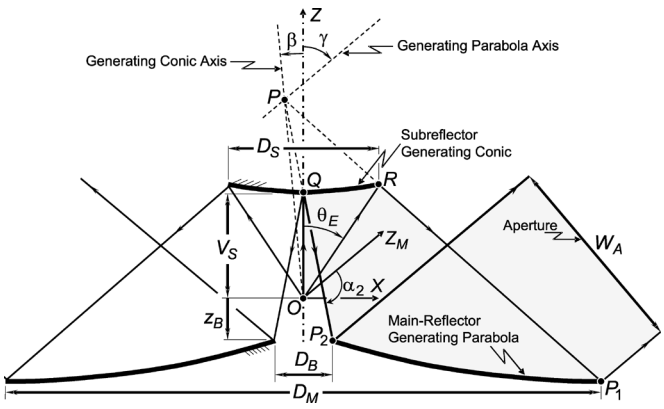

Fig. 2. Basic parameters of an omnidirectional dual-reflector system for option II.

in Section III by applying the formulation in the synthesis of omnidirectional dual-reflector arrangements. The case studies explore the potentialities of these configurations as base-station antennas in point–multipoint radio links with a tilted main lobe. In order to estimate the limits for applicability of the proposed design procedure, the antennas are analyzed by the method of moments (MoM) technique.

II. Antenna Geometry

The present antennas are composed of two reflectors, which are bodies of revolution with a common symmetry axis (the z axis), as depicted in Figs. 1 and 2 for the two possible ray-mapping options. The subreflector can be generated by any conic section, which is connected to the symmetry axis at point Q. This point defines the vertex of the subreflector surface, where a curvature discontinuity is generally present. In turn, the main reflector is generated by a parabola, which is limited by points P_1 and P_2 defining the main-reflector outer and inner rims, respectively. P_2 can be placed out of the symmetry axis, leaving space for the feed access to the principal focus (O) of the dual-reflector system (see Figs. 1 and 2). As an illustration, Fig. 3 depicts a three-dimensional (3-D) view of the dual-reflector arrangement generated by the conics of Fig. 1.

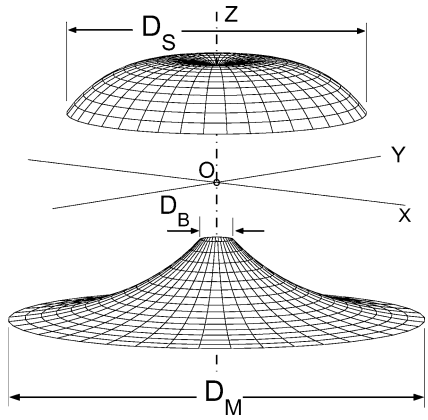

Fig. 3. Three-dimensional view of the omnidirectional dual-reflector antenna generated by the conics of Fig. 1.

The subreflector generating conic has two focci, located at points O and P (see Figs. 1 and 2). Point O is at the symmetry axis and defines the antenna principal focus, while P is positioned to coincide with the focus of the main-reflector generating parabola, so that a ray departing from O reaches the antenna aperture (after two reflections) parallel to the parabola axis, according to GO principles. Consequently, after the rotation of the generating conics about the symmetry axis to form the reflector surfaces (as depicted in Fig. 3), a spherical wavefront emanating from O is transformed into a conical wavefront at the antenna aperture (see Figs. 1 and 2). According to Malus' theorem, the phase distribution over this conical aperture is uniform. Consequently, if amplitude and polarization nonuniformities at the aperture are sufficiently small, the antenna main-beam direction in the elevation plane is approximately given by the angle γ that the parabola axis makes with the antenna symmetry axis (see Figs. 1 and 2). For instance, if $\gamma = \pi/2$, the present reflector arrangements correspond to those investigated in [6]–[8], with broadside radiation patterns.

As previously mentioned, there are two different ray-mapping options. The first one (hereinafter named option I) provides the converse of the feed illumination toward the antenna aperture; i.e., the principal feed ray, departing from O along the symmetry axis ($\theta_F = 0$), is directed toward P_1 after the first reflection, as depicted in Fig. 1. The second mapping option (option II) has the feed principal ray reflected toward P_2 (see Fig. 2). For each mapping option, there are two different configurations (totalizing four different dual-reflector arrangements), depending on the location of the ring caustic defined by P after rotation about the symmetry axis. If P lies between the sub- and main reflectors, the corresponding ring caustic is real. On the contrary, the ring caustic is virtual. Consequently, a certain mapping option has a real or a virtual ring caustic (the geometrical features will be discussed in Section II-C). Furthermore, with respect to the omnidirectional reflector arrangements with $\gamma = \pi/2$ described in [8], the omnidirectional axis-displaced ellipse (OADE, which has a real ring caustic) and hyperbola (OADH, with virtual ring caustic) are particular cases of option I, while the omnidirectional axis-displaced Cassegrain (OADC, with virtual ring caustic) and Gregorian (OADG, with real ring caustic) are examples of the option II.

A. Input Parameters

In order to uniquely specify an omnidirectional dual-reflector arrangement, six geometric parameters are needed, besides the choice of the desired mapping option: the focal length (F) of the generating parabola and the tilt angle (γ) between its axis and the symmetry axis, the eccentricity (e) and the interfocal distance $(2c = |\overline{OP}|)$ of the subreflector's generating conic and the tilt angle (β) between its axis and the symmetry axis, and the antenna aperture limits, which can be specified by the subreflector edge angle (θ_E) or, conversely, by the width of the antenna conical aperture (W_A). Most of these parameters are depicted in Figs. 1 and 2. However, the above parameters are not useful in practical designs, as the geometric specifications for reflector antennas are commonly given in terms of volumes, diameters, etc. In order to attain a general design procedure grounded on practical antenna dimensions, the six input parameters used for the dual-reflector synthesis are those related to the location of points Q, P_1, and P_2 with respect to O (which is the origin of the coordinate systems to be adopted) plus the angle γ (which approximately provides the main-beam direction of the antenna radiation pattern in the elevation plane).

Here, a point will be located by its corresponding position vector, always with respect to O. For instance, the subreflector vertex Q is located by (see Figs. 1 and 2)

$$\vec{Q} = V_S \hat{z} \tag{1}$$

where the input parameter V_S, in practice, defines the distance between the feed phase-center (at O) and the subreflector vertex. The generating-parabola extremes are described by

$$\vec{P}_1 = \frac{D_M}{2}\hat{x} + \left[z_B + \left(\frac{D_M - D_B}{2}\right)\cot\gamma - W_A \csc\gamma\right]\hat{z} \tag{2}$$

$$\vec{P}_2 = \frac{D_B}{2}\hat{x} + z_B\hat{z} \tag{3}$$

where D_M is the diameter of the main-reflector outer rim, and z_B and D_B are the z coordinate and diameter of the main-reflector central opening, respectively, as illustrated in Figs. 1 and 2. Note that z_B and D_B control the feed access to the focal point O. Consequently, the six input parameters are W_A, D_M, D_B, z_B, V_S, and γ, always with $\gamma \neq 0$. For directional axis-displaced dual-reflector antennas (i.e., $\gamma = 0$), the design procedure to be used is that of [9].

It is important to observe that, in this paper, positive (negative) angles are depicted with a counterclockwise (clockwise) orientation in the figures in order to establish uniform design equations. The design procedure is discussed next in terms of the vector components of $\vec{Q}$, $\vec{P}_1$, and $\vec{P}_2$. One must then observe that the success of the design also depends on the relative location of Q, P_1, and P_2. For example, if $z_B > 0$, then one must judiciously choose D_B to prevent feed rays from being blocked by the back of the main reflector before reaching the subreflector.

B. Design Equations

The procedure starts with the definition of the parabola geometric features. For that, an auxiliary coordinate system x_M, z_M is defined, with its origin still at O (see Figs. 1 and 2). Such a coordinate system is rotated by γ with respect to the principal coordinate system x, z such that the z_M axis is parallel to the parabola axis. Consequently, the unit directions $\hat{x}_M$ and $\hat{z}_M$ are given by

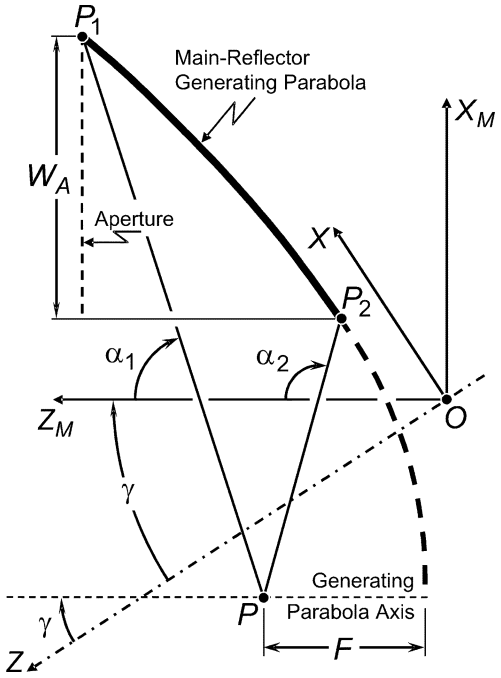

Fig. 4. Basic parameters of the main-reflector generating parabola.

$$\hat{x}_M = \cos\gamma\hat{x} - \sin\gamma\hat{z} \tag{4}$$

$$\hat{z}_M = \sin\gamma\hat{x} + \cos\gamma\hat{z}. \tag{5}$$

The auxiliary coordinate system and some pertinent geometric parameters are properly illustrated in Fig. 4.

We then proceed to determine $\vec{P}$, which locates the parabola's focal point P. It can be shown from the parabola's polar equation that

$$\vec{P}_1 - \vec{P} = 2F\left[\eta(\alpha_1)\hat{x}_M + \frac{\eta^2(\alpha_1) - 1}{2}\hat{z}_M\right] \tag{6}$$

$$\vec{P}_2 - \vec{P} = 2F\left[\eta(\alpha_2)\hat{x}_M + \frac{\eta^2(\alpha_2) - 1}{2}\hat{z}_M\right] \tag{7}$$

where

$$\eta(x) = \cot\left(\frac{x}{2}\right) \tag{8}$$

and the auxiliary angles α_1 and α_2 are as illustrated in Figs. 1, 2, and 4. From (6) and (7)

$$\vec{P}_1 - \vec{P}_2 = 2F\left[\eta(\alpha_1) - \eta(\alpha_2)\right]\left[\hat{x}_M + \frac{\eta(\alpha_1) + \eta(\alpha_2)}{2}\hat{z}_M\right] \tag{9}$$

observing that $\vec{P}_1 - \vec{P}_2$ is a known vector. So, from (9), one can show that

$$\eta(\alpha_1) + \eta(\alpha_2) = \frac{2\hat{z}_M \cdot (\vec{P}_1 - \vec{P}_2)}{\hat{x}_M \cdot (\vec{P}_1 - \vec{P}_2)} \tag{10}$$

which relates α_1 and α_2 to each other. However, one of these angles is known from the given input parameters. Observe from Figs. 1 and 2, which illustrate the mapping options I and II, respectively, that

$$\frac{(\vec{P}_i - \vec{Q})}{|\vec{P}_i - \vec{Q}|} = \sin\alpha_i \hat{x}_M + \cos\alpha_i \hat{z}_M = \frac{2\eta(\alpha_i)\hat{x}_M + \left[\eta^2(\alpha_i) - 1\right]\hat{z}_M}{1 + \eta^2(\alpha_i)} \quad (11)$$

where $\alpha_i = \alpha_1$ or α_2 for option I or II, respectively. Consequently

$$\eta(\alpha_i) = \frac{\hat{x}_M \cdot (\vec{P}_i - \vec{Q})}{|\vec{P}_i - \vec{Q}| - \hat{z}_M \cdot (\vec{P}_i - \vec{Q})}. \quad (12)$$

The other auxiliary angle is immediately obtained from (10) and $\vec{P}$ is further defined from (6) or (7), with the help of (9). From (9), one also obtains the parabola focal length

$$F = \frac{\hat{x}_M \cdot (\vec{P}_1 - \vec{P}_2)}{2\left[\eta(\alpha_1) - \eta(\alpha_2)\right]} = \frac{\hat{z}_M \cdot (\vec{P}_1 - \vec{P}_2)}{\eta^2(\alpha_1) - \eta^2(\alpha_2)}. \quad (13)$$

Observing that $\vec{P}$ is known by this time, we now proceed to establish the parameters of the subreflector generating conic. The interfocal distance $2c$ is immediately attained from

$$2c = |\overline{OP}| = |\vec{P}| \quad (14)$$

while the angle β between the conic axis and the symmetry axis is obtained without quadrant ambiguity from (see Figs. 1 and 2)

$$\vec{P} = 2c(\sin\beta\hat{x} + \cos\beta\hat{z}). \quad (15)$$

Finally, the eccentricity e is determined from the conic equation

$$\frac{2c}{e} = \hat{z} \cdot \vec{Q} + (\vec{P} - \vec{Q}) \cdot \frac{(\vec{P}_i - \vec{Q})}{|\vec{P}_i - \vec{Q}|} \quad (16)$$

where $\vec{P}_i = \vec{P}_1$ or $\vec{P}_2$ for option I or II, respectively. It is important to emphasize that (16) may (correctly) provide negative values for the ratio $2c/e$, depending on the location of the ring caustic P.

With the conic parameters specified for a given mapping option (I or II), the generating conics and, consequently, the dual-reflector surfaces are uniquely determined. Before presenting some geometrical features of the several dual-reflector configurations, it is interesting to provide equations for the subreflector edge angle (θ_E) and diameter (D_S), which are useful parameters for the antenna design. Both are specified by the vector $\vec{R}$, which locates the point R corresponding to the subreflector rim (see Figs. 1 and 2). From the conic polar equation, one can show that

$$\vec{R} = \vec{P} + \frac{(c/e)(e^2 - 1)\left[\sin(\alpha_j + \gamma)\hat{x} + \cos(\alpha_j + \gamma)\hat{z}\right]}{1 - e\cos(\alpha_j + \gamma - \beta)} \quad (17)$$

where $\alpha_j = \alpha_2$ or α_1 for option I or II, respectively. Then, θ_E and D_S are directly obtained from

$$\tan\theta_E = \frac{\hat{x} \cdot \vec{R}}{\hat{z} \cdot \vec{R}} \quad (18)$$

$$D_S = 2|\hat{x} \cdot \vec{R}|. \quad (19)$$

It is important to stress that (17) may provide $\hat{x} \cdot \vec{R} < 0$ and, consequently, $\theta_E < 0$.

C. Geometrical Features

As previously mentioned, each mapping option can be further classified into two different configurations, depending on the location of the ring caustic (defined by P). There are several ways of visualizing such configurations, but here we prefer to do so by exploring the location of P with respect to Q (see Figs. 1 and 2).

We start with option I. Several different configurations, in a pertinent ordering, are qualitatively illustrated in Fig. 5 for an arbitrary angle γ. Fig. 5(a) shows a configuration where the ring caustic P is real (i.e., located between the reflectors). Note that the subreflector generating conic is an ellipse and the edge angle θ_E is positive. Besides the (real) ring caustic, the subreflector also has a (virtual) line caustic over the symmetry axis (as the subreflector is a body of revolution) and, consequently, the ray tube reflected by the subreflector has an astigmatic wavefront. By changing the input parameters (for instance, by increasing V_S), one can come up with dual-reflector systems similar to that of Fig. 5(a) (i.e., with a real ring caustic and a virtual line caustic) with P continuously approaching Q.

The situation where $P = Q$ and, consequently, $\theta_E = 0$ represents the turning point between the two different configurations of option I. The other configuration, like that of Fig. 5(b), has a virtual ring caustic (P surpasses Q, appearing *above* the subreflector) and a real line caustic (over the symmetry axis and between the reflectors), with $\theta_E < 0$. Initially, the subreflector is generated by the hyperbola's branch closest to focus P. It is possible, however, to continuously increase the distance between P and Q, so to have the configuration of Fig. 5(c) (still with a virtual ring caustic and real line caustic). Now, the subreflector is generated by the hyperbola's branch closest to O, $F \to \infty$ and, consequently, the generating parabola tends to a straight line. Finally, it is possible to have P *below* the main reflector, as depicted in Fig. 5(d) (still with a virtual ring caustic and real line caustic). Now, the subreflector conic is an ellipse, $F < 0$ and, consequently, the curvature of the main-reflector parabola is reversed. It is interesting to observe that, with $\gamma = \pi/2$, the geometry corresponding to Fig. 5(a) is classified as an OADE in [8], while those of Fig. 5(b)–(d) are classified as OADH [8].

The configurations corresponding to option II are illustrated in Fig. 6. We start with Fig. 6(a), where P lies between the reflectors and, consequently, the subreflector is generated by an ellipse, with $\theta_E < 0$. Such configuration has a subreflector with real ring and line caustics, which never occurs for the option I geometries previously discussed. By appropriately changing the input parameters, one can design a dual-reflector system where P approaches Q. As for option I, the turning point occurs at $P = Q$. After that, the configuration (now with $\theta_E > 0$) has virtual ring and line caustics, as in Fig. 6(b). In this figure, P

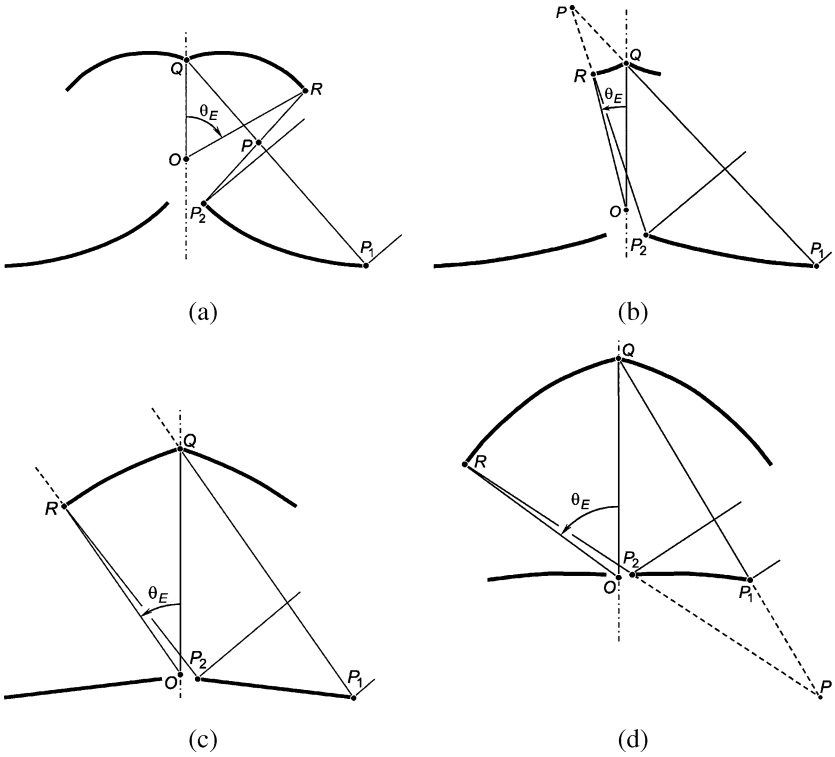

Fig. 5. Some different configurations for the option I.

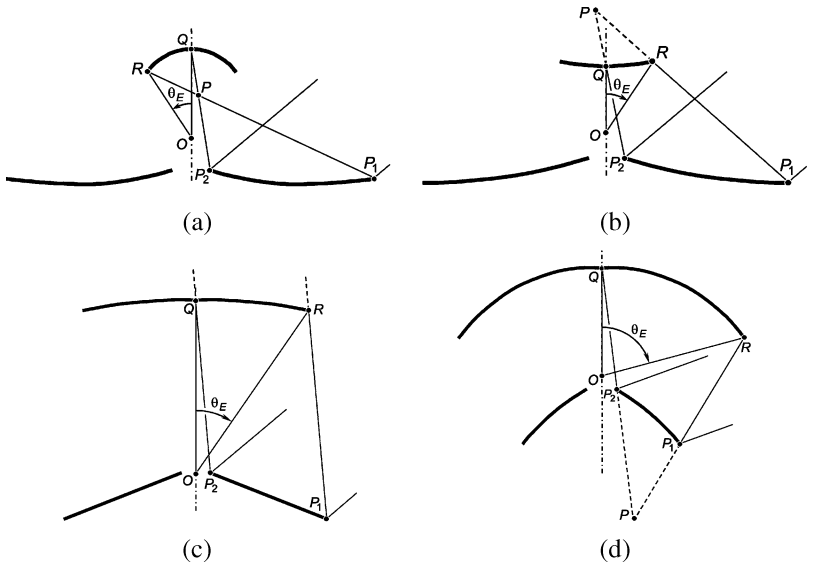

Fig. 6. Some different configurations for the option II.

appears *above* the subreflector, which is generated by the hyperbola's branch closest to P. As P is moved away from Q, the subreflector eventually starts to be generated by the other hyperbola's branch and, in the limit $F \to \infty$, the main-reflector parabola becomes a straight line, as depicted in Fig. 6(c). Finally, P can be located *below* the main reflector, as in Fig. 6(d). Now the main-reflector parabola has a reversed curvature (i.e., $F < 0$) and the subreflector conic is an ellipse. But both ring and line caustics of the subreflector are still virtual. For $\gamma = \pi/2$, the configuration corresponding to Fig. 6(a) is classified as an OADG in [8], while those of Fig. 6(b)–(d) are classified as OADC [8].

D. Maximum Directivity

Before proceeding to the case studies, we shall present useful upper-bound formulas for estimating the maximum directivity attained by such omnidirectional dual-reflector antennas. Following the procedure in [4] and for $60^\circ < \gamma < 120^\circ$, the

far-zone linearly polarized electric field radiated by the antenna conical aperture is approximately given by

$$E(\theta) \approx B(\theta)U(\theta)\frac{e^{-jkr}}{r} \tag{20}$$

where

$$B(\theta)=\frac{jkx_o}{2}\left[\sin\theta J_0(kx_o\sin\theta)+j\sin\gamma J_1(kx_o\sin\theta)\right] \tag{21}$$

$$U(\theta)=e^{jkz_o}\int_{-W_A/(2\sin\gamma)}^{W_A/(2\sin\gamma)} E_A(\ell)e^{jk(\cos\gamma-\cos\theta)\ell}d\ell \tag{22}$$

E_A is the linearly-polarized geometrical-optics electric field at the antenna aperture, x_o and z_o are the x and z coordinates of the aperture central point, and J_0 and J_1 are the Bessel functions of order 0 and 1, respectively. One can show that $|B(\theta)|$ is quite uniform around $\theta \approx \gamma$ if $60^\circ < \gamma < 120^\circ$. So, the main-beam peak is defined by $|U(\theta)|$ and will occur at $\theta \approx \gamma$ if E_A has negligible variation over the aperture. Under these circumstances and assuming E_A uniform at the aperture, one can show that the maximum directivity D_o at $\theta = \gamma$ is given by

$$D_o = \frac{k^2 W_A x_o}{2}\left[J_0^2(kx_o\sin\gamma)+J_1^2(kx_o\sin\gamma)\right]. \tag{23}$$

If $kx_o\sin\gamma \gg 1$, one can show from the asymptotic expansion of Bessel functions for large arguments that

$$D_o \approx \frac{2W_A}{\lambda\sin\gamma} \tag{24}$$

which provides an upper bound for the maximum directivity of the omnidirectional dual-reflector antenna.

III. Case Studies

In order to illustrate the design procedure discussed in Section II, some case studies are investigated, covering both ray-mapping options. The antenna configurations were initially established with $\gamma = 90^\circ$ (i.e., with a broadside radiation pattern), with the help of the studies conducted in [7] and [8] to specify antenna geometries with high radiation efficiencies. Afterwards, the broadside arrangements were slightly changed to provide omnidirectional dual-reflector antennas with $\gamma = 90^\circ \pm 12^\circ$ in order to illustrate the potentialities of the present configurations as base-station antennas in point–multipoint microwave and millimeter-wave radio links. For each antenna investigated in this section, a full-wave analysis based on the MoM technique was conducted to validate the design procedure.

The feed to be employed in these antennas has to provide a circularly symmetric radiation pattern. For vertical polarization, a pure radial-mode aperture such as a TEM coaxial horn or a TM_{01} excited conical horn can provide the desired radiation pattern with a null in the z axis [1]–[8]. Here, the feed adopted in all case studies is a TEM coaxial horn with internal and external radii $r_i = 0.4\lambda$ and $r_e = 1\lambda$, respectively, at the horn's aperture. As r_i and r_e are relatively small, the phase center of the horn's far-zone radiation is located very close to the horn's aperture. Consequently, such aperture was placed at the antenna focal plane, which, in turn, was set to coincide with the plane of the main-reflector central opening (i.e., $z_B = 0$ in Figs. 1 and 2), providing a compact arrangement that properly accommodates the horn's structure.

The first configurations to be investigated correspond to option I. In order to provide a half-power beamwidth with approximately 10°, an aperture width $W_A = 7\lambda$ was chosen. To appropriately accommodate the feed structure, $z_B = 0$ (as previously explained) and $D_B = 2.4\lambda$, leaving sufficient space for the horn's aperture. Then, given the feed geometry and for $\gamma = 90^\circ$, the results in [7] and [8] were applied to attain a (theoretically) highly efficient configuration with $D_M = 17.56\lambda$ and $V_S = 7.11\lambda$. As explained in Section II, these input parameters uniquely define the omnidirectional dual-reflector arrangement. Furthermore, one can show from (18) and (19) that $\theta_E = 55^\circ$ and $D_S = 14\lambda$. Afterwards, the input parameter γ was changed to 78°, but still with $W_A = 7\lambda$ (to provide a similar aperture geometry), $D_M = 17.56\lambda$ (to approximately maintain the overall antenna volume), $\theta_E = 55^\circ$ (to basically provide the same feed spillover), $z_B = 0$, and $D_B = 2.4\lambda$. With the help of the formulation of Section II, one can show that this is accomplished with $V_S = 6.61\lambda$ and, from (19), $D_S = 13.35\lambda$. For such arrangement, (23) estimates $D_o = 11.6$ dB. The antenna and its radiation pattern are depicted in Fig. 7(a) and (c), respectively, from where one observes that the MoM analysis predicts a gain $G_o = 9.97$ dBi at $\theta \approx 78^\circ$, considering feed return loss and spillover. Some geometrical parameters, including those of the conic sections, are listed in Table I.

Then, in order to set $\gamma = 102^\circ$ while sustaining the values of W_A, D_M, θ_E, z_B, and D_B adopted previously, one must choose $V_S = 7.64\lambda$, which provides $D_S = 14.71\lambda$. This particular antenna and its radiation pattern are illustrated in Fig. 7(b) and (c), respectively, while some geometrical parameters are listed in Table I. From Fig. 7(c), one observes that $G_o = 9.83$ dBi at $\theta \approx 102^\circ$ [from (23), one obtains $D_o = 11.6$ dB]. The antennas of Fig. 7(a) and (b) can, in principle, provide similar illuminations in the elevation plane, for example, by turning that of Fig. 7(a) upside down. Therefore, it is interesting to point out from Table I that the configuration with $\gamma = 78^\circ$ has a subreflector that is slightly smaller and closer to the main reflector than the subreflector of the antenna with $\gamma = 102^\circ$, indicating that the former is more compact than the later, as one can inspect from Fig. 7(a) and (b).

The last case studies comprise antennas of the mapping option II. To render proper comparisons among the several configurations investigated in the present section, the values of $W_A = 7\lambda$, $D_M = 17.56\lambda$, $D_B = 2.4\lambda$, $z_B = 0$, and $\theta_E = 55^\circ$ are adopted once more for two different geometries: with $\gamma = 78^\circ$ and 102°, as before. The dual-reflector antennas are fed by the previous TEM coaxial horn (with $r_i = 0.4\lambda$ and $r_e = 1\lambda$). The option II configurations with $\gamma = 78^\circ$ and 102° were obtained by choosing $V_S = 7.63\lambda$ and 8.46λ, respectively. Their geometries are depicted in Fig. 8(a) and (b), respectively, and their radiation patterns are illustrated in Fig. 8(c) [from (23), one obtains $D_o = 11.6$ dB for both antennas]. Their geometrical features are listed in Table I. As for option I, the antenna

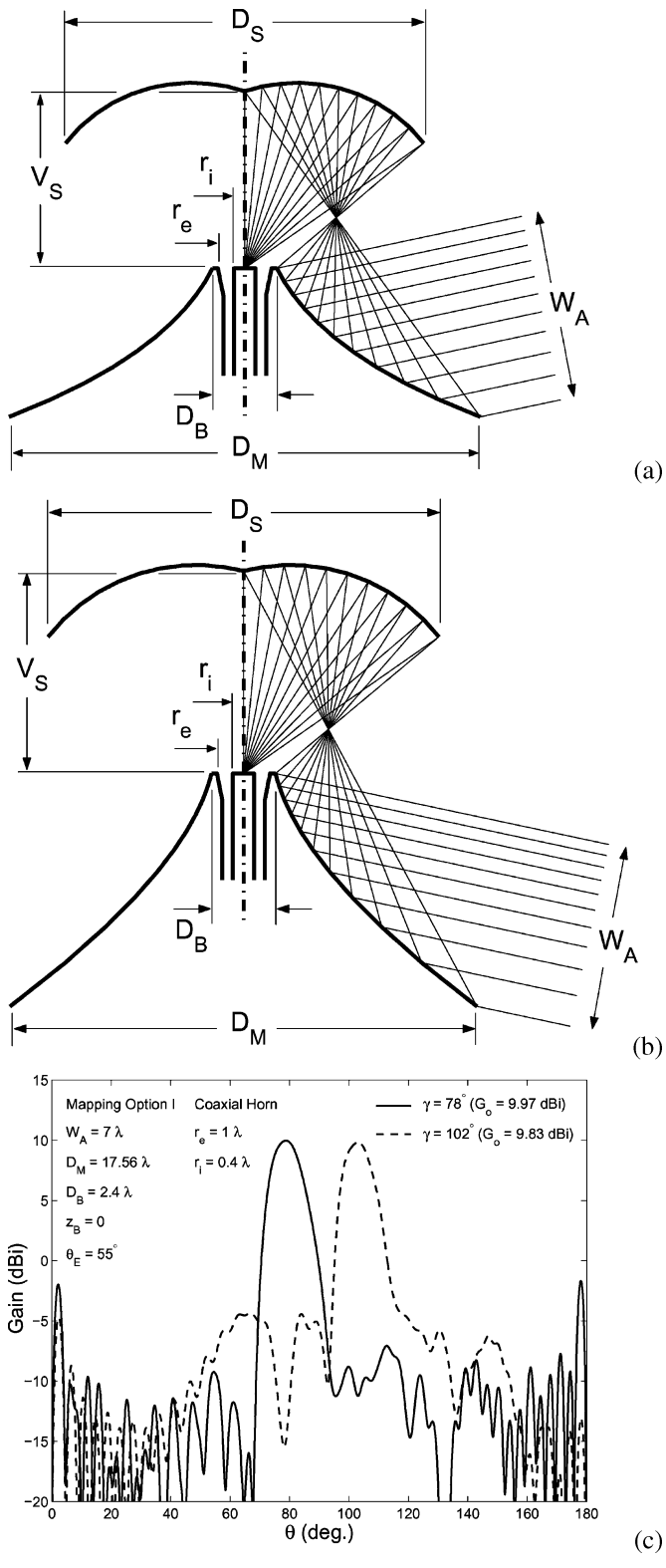

Fig. 7. Option I omnidirectional dual-reflector antennas with $W_A = 7\lambda$, $D_M = 17.56\lambda$, $D_B = 2.4\lambda$, $z_B = 0$, and $\theta_E = 55°$, fed by a TEM coaxial horn with $r_e = 1\lambda$ and $r_i = 0.4\lambda$: draws of the antennas with (a) $\gamma = 78°$ and (b) $102°$, plus (c) radiation patterns in the elevation plane from MoM analyses.

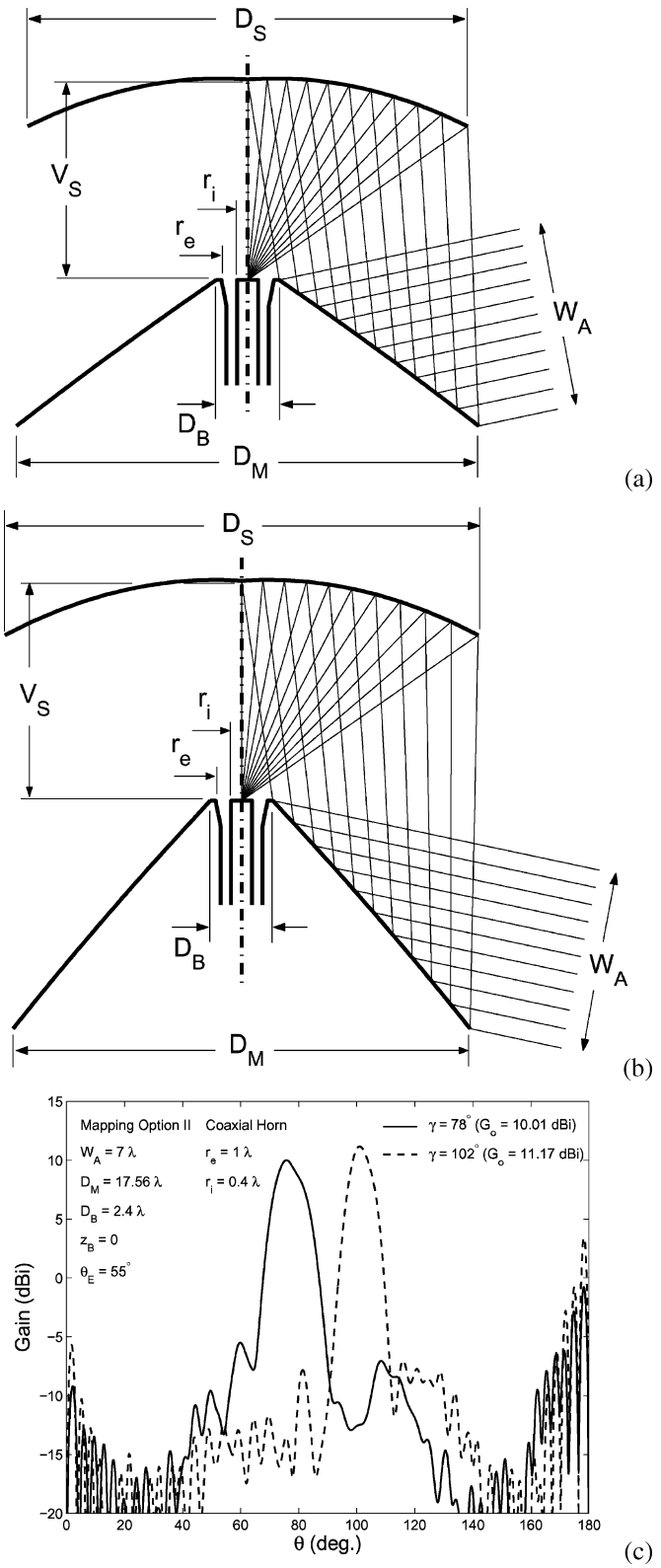

Fig. 8. Option II omnidirectional dual-reflector antennas with $W_A = 7\lambda$, $D_M = 17.56\lambda$, $D_B = 2.4\lambda$, $z_B = 0$, and $\theta_E = 55°$, fed by a TEM coaxial horn with $r_e = 1\lambda$ and $r_i = 0.4\lambda$: draws of the antennas with (a) $\gamma = 78°$ and (b) $102°$, plus (c) radiation patterns in the elevation plane from MoM analyses.

with $\gamma = 78°$ is more compact than that with $\gamma = 102°$, for which $D_S > D_M$ [see Fig. 8(b)].

Finally, from the results presented in Figs. 7 and 8 and Table I, one concludes that the mapping option I can yield omnidirectional configurations that are slightly more compact than those of option II; but the former may provide slightly higher gains than the later, as already observed in [7] and [8] for $\gamma = 90°$.

TABLE I
SOME GEOMETRICAL FEATURES AND MAXIMUM GAIN (G_o) OF THE OMNIDIRECTIONAL DUAL-REFLECTOR ANTENNAS OF THE CASE STUDIES

Option	I		II	
γ	78°	102°	78°	102°
$W_A(\lambda)$	7	7	7	7
$D_M(\lambda)$	17.56	17.56	17.56	17.56
$D_B(\lambda)$	2.4	2.4	2.4	2.4
$z_B(\lambda)$	0	0	0	0
$V_S(\lambda)$	6.61	7.64	7.63	8.46
$D_S(\lambda)$	13.35	14.71	16.72	18.19
θ_E	55°	55°	55°	55°
$F(\lambda)$	2.73	2.10	-32.7	-15.8
$2c(\lambda)$	3.90	3.60	62.3	48.4
e	0.3135	0.2502	0.8043	0.7420
β	61.0°	62.4°	170.0°	170.5°
G_o(dBi)	9.97	9.83	10.01	11.17

IV. CONCLUSION

This paper presented closed-form equations for the geometric-optics design of axis-displaced dual-reflector antennas suited for an omnidirectional coverage with an arbitrary main-beam direction in the elevation plane. The formulation covers all possible classical configurations in a uniform treatment, enabling a proper investigation of the geometrical features among the several configurations.

Several case studies, covering different dual-reflector compact arrangements, were investigated and analyzed by the method of moments technique in order to demonstrate the usefulness of the present formulation for design purposes. The investigation also showed that the present dual-reflector antennas can provide relatively high gains together with an omnidirectional coverage, being consequently suited for use at base stations of microwave and millimeter-wave radio links.

REFERENCES

[1] A. P. Norris and W. D. Waddoup, "A millimetric wave omnidirectional antenna with prescribed elevation shaping," in *Proc. 4th Int. Conf. Antennas Propagation (ICAP)*, 1985, pp. 141–145.

[2] M. Orefice and P. Pirinoli, "Dual reflector antenna with narrow broadside beam for omnidirectional coverage," *Electron. Lett.*, vol. 29, no. 25, pp. 2158–2159, Dec. 9, 1993.

[3] P. Besso, R. Bills, P. Brachat, and R. Vallauri, "A millimetric wave omnidirectional antenna with cosecant squared elevation pattern," in *Proc. 10th Int. Conf. Antennas Propagation (ICAP)*, 1997, vol. 1, pp. 448–451.

[4] A. G. Pino, A. M. A. Acuña, and J. O. R. Lopez, "An omnidirectional dual-shaped reflector antenna," *Microw. Opt. Tech. Lett.*, vol. 27, no. 5, pp. 371–374, Dec. 5, 2000.

[5] J. R. Bergmann, F. J. V. Hasselmann, and M. G. C. Branco, "A single-reflector design for omnidirectional coverage," *Microwave Opt. Tech. Lett.*, vol. 24, no. 6, pp. 426–429, March 20, 2000.

[6] J. R. Bergmann and F. J. S. Moreira, "An omni directional ADE reflector antenna," *Microwave Opt. Tech. Lett.*, vol. 40, no. 3, pp. 250–254, Feb. 5, 2004.

[7] J. R. Bergmann and F. J. S. Moreira, "Simple design equations for omnidirectional axis-displaced dual-reflector antennas," *Microw. Opt. Tech. Lett.*, vol. 45, no. 2, pp. 159–163, Apr. 20, 2005.

[8] F. J. S. Moreira and J. R. Bergmann, "Classical axis-displaced dual-reflector antennas for omnidirectional coverage," *IEEE Trans. Antennas Propag.*, vol. 53, no. 9, pp. 2799–2808, Sep. 2005.

[9] F. J. S. Moreira and A. Prata, Jr., "Generalized classical axially symmetric dual-reflector antennas," *IEEE Trans. Antennas Propag.*, vol. 49, no. 4, pp. 547–554, Apr. 2001.

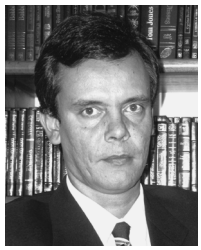

Fernando José da Silva Moreira (S'89–M'98) was born in Rio de Janeiro, Brazil, in 1967. He received the B.S. and M.S. degrees in electrical engineering from the Catholic University, Rio de Janeiro, Brazil, in 1989 and 1992, respectively, and the Ph.D. degree in electrical engineering from the University of Southern California, Los Angeles, in 1997.

Since 1998, he has been with the Department of Electronics Engineering of the Federal University of Minas Gerais, Belo Horizonte, Brazil, where he is currently an Associate Professor. His research interests are in the areas of electromagnetics, antennas, and propagation. He has authored or coauthored over 60 journal and conference papers in these areas.

Dr. Moreira is a member of Eta Kappa Nu and the Brazilian Microwave and Optoelectronics Society.

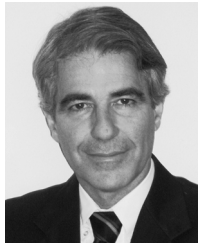

José Ricardo Bergmann (M'88) received the Electrical Engineering degree from the Universidade Federal do Rio Grande do Sul, Brazil, in 1975, the M.Sc. degree in electrical engineering from the Instituto Militar de Engenharia, Brazil, in 1979, and the Ph.D. degree in electrical engineering from Queen Mary College, University of London, London, U.K., in 1986.

Currently, he is Associated Professor and Head of the Antenna Group of the Center of Telecommunications Studies (CETUC) at the Catholic University of Rio de Janeiro, Brazil, where he has been Associate Vice-President for Academic Affairs—Research and Postgraduate of the Catholic University of Rio de Janeiro since 1998. His research interests comprise numerical modeling, synthesis and analysis of reflector systems.

Dr. Bergmann was Vice-President and President of the Brazilian Microwave and Optoelectronics Society (SBMO) from 1996 to 2000.